http://dx.doi.org/10.5012/bkcs.2014.35.4.1091

Synthesis, Structural Characterization, and Catalytic Activity of Flower Like ZnO Nanostructures

K. Ramachandran, G. Gnana Kumar,[*] Ae Rhan Kim,[†] and Dong Jin Yoo[‡,*]

Department of Physical Chemistry, School of Chemistry, Madurai Kamaraj University, Madurai-625021, India
[*]E-mail: kumarg2006@gmail.com
[†]Department of Chemistry, Chonbuk National University, Jeollabuk-do 561-756, Korea
[‡]Specialized Graduate School of Hydrogen and Fuel Cells Engineering, Hydrogen and Fuel Cell Research Center, Chonbuk National University, Jeollabuk-do 561-756, Korea. [*]E-mail: djyoo@jbnu.ac.kr
Received November 7, 2013, Accepted December 17, 2013

Tageteserecta flower like zinc oxide nanostructures composed of hexagonal nanorods were synthesized *via* sonochemical method at room temperature. The synthesized nanomaterials exhibited wurtzite hexagonal phase structure with the single crystalline nature. The diameter of the individual nanorods that constitute the flower shaped zinc oxide structures is in the range of 120-160 nm. The sonication time effectively determined the morphological properties of the prepared materials. The catalytic activity of prepared zinc oxide nanostructures towards *N*-formylation reactions were evaluated without any surface modification and the nanostructures exhibited good reaction yield with the prompt recyclability behavior.

Key Words : Activity, Adsorption, Nanocatalyst, X-ray diffraction, Zinc oxide

Introduction

N-Formylation reaction has been considered as a most significant reaction in synthetic organic chemistry. Formamides exhibit potential applications in the synthesis of pharmaceutical compounds such as fluoroquinolines,[1] substituted aryl imidazoles,[2] 1,2-dihydroquinolines,[3] nitrogen-bridged heterocycles[4] *etc*., Formamides also find its applications in Vilsmeier formylation,[5] preparation of isocyanide,[6] Lewis base organic transformation, allylation and reduction reactions. Formyl group is highly useful as an amino protecting group in peptide synthesis. Hence, extensive research efforts were devoted to develop the time and cost efficient strategic techniques for the synthesis of various amide derivatives.[3-5] However, the reported *N*-formylation methods exhibited certain bottlenecks such as sensitive to atmospheric moisture, toxic formylating agents, high temperature, prolonged reaction times for completion, severe reaction conditions, by-products, thermal instability of products *etc*.,[3-5] which collectively faded the large scale applications of amide derivatives. To eradicate the aforementioned significant issues, the reaction of formic acid with amine derivatives has been proposed. The yield of *N*-formylation reaction could be further enhanced by bringing the reactants in a closer proximity and proper orientation. The nanometric metal and metal oxides catalyzed organic reactions are aimed at the above. Among the number of nanometric heterogeneous metal and metal oxide catalysts used in organic catalytic reactions, zinc oxide (ZnO) is well known for its nontoxic, inexpensive, less hygroscopic and corrosive, easier isolation, prompt recyclability and simple disposal behaviors.[7-11]

One-dimensional (1D) ZnO nanostructures have received tremendous attention owing to their significant properties in basic scientific research and their unique applications in nanoscale devices.[7] Their direct wide band gap (3.37 eV) at room temperature, large saturation velocity (3.2×10^7 cm/s), high breakdown voltage, large exciton binding energy, piezoelectric, and biocompatibility ensured its versatile applications in number of fields.[8-11] The aforementioned unique properties of ZnO are purely dependent on its surface, controlled morphology and particle size. Hence, variety of ZnO nanostructures was synthesized with the aid of number of physical and chemical techniques.[12-14] Among the several nanostructures of ZnO, flower shaped structures are highly attractive due to its promising catalytic activities.[15] Flower shaped nanostructures exhibited superior catalytic performances over their spherical counterparts which is attributed to its high specific surface area.[16] The hyper-branched network of flower like ZnO nanostructures played a vital role in the determination of effectual catalytic active sites.[17] Hence, the synthesis of flower like ZnO is field of interest and various techniques such as thermal evaporation, cyclic feeding chemical vapor deposition, chemical vapor deposition (CVD), spray pyrolysis, ion beam assisted deposition, laser-ablation, sputter deposition, template assisted growth metal–organic CVD[18-21] *etc*., were exploited for the synthesis of flower shaped ZnO nanostructures. Though the aforementioned methods were effectual in synthesizing flower shaped ZnO structures, their tedious preparation method, time consumption, need of sophisticated accessories and high cost hindered the large scale applications of ZnO.[18-21] It enunciates the need of a new method which can produce such structures, without using metal catalysts or templates, with better crystal quality preferably at lower temperature.

In recent years, sonochemical process has been proven to be a powerful technique for the synthesis of novel nano-

metric materials with the desired properties.[22] The chemical effects of ultrasound arise from acoustic cavitation *i.e.*, the formation, growth, and implosive collapse of bubbles in a liquid. The implosive collapse of bubble generates localized hot spots through the adiabatic compression or shock wave formation within the gas phase of the collapsing bubble which is very useful in synthesizing the novel nanometric materials.[23-24] The easier availability of accessories, effortless preparation, less time consumption and affordable cost promote the competence of sonication chemistry further. Highly crystalline ZnO nanospheres were synthesized with the aid of sonochemical method.[25] The sonochemical synthesis of ZnO-poly vinyl alcohol composite was also reported.[26,27] ZnO hollow spheres were prepared by sonochemical method using monosaccharides as templates.[28] Hu *et al.* reported the ZnO nanorods using zinc nitrate and hexamethylenetetramine at 90 °C.[29] Though the aforementioned efforts were reported on the preparation of nanometric ZnO using sonochemical process, sonochemical synthesis of flower shaped ZnO nanostructures without the aid of additives have not been reported yet. Herein, we report the synthesis and catalytic activity of flower shaped ZnO composed of hexagonal nanorods towards the *N*-formylation reactions under solvent free conditions.

Materials and Methods

Materials. Zinc acetate dihydrate ($Zn(CH_3COO)_2{\cdot}2H_2O$), sodium hydroxide (NaOH), sodium bicarbonate ($NaHCO_3$), sodium sulfate (Na_2SO_4), ethyl acetate, $CDCl_3$ and DMSO-d_6 were derived from Aldrich Chemical Corporation and used without further purification. Formic acid and various aniline derivatives were also purchased from Aldrich Chemical Corporation.

Characterizations. Morphological images of the prepared ZnO nanostructures were examined by using a JSM-6400 field emission scanning electron microscopy (JEOL, Japan). The specific surface areas of the prepared nanostructures were obtained by using a Brunauer–Emmett–Teller (BET) surface area analyzer (Belsorp). Conventional TEM micrograph was recorded on a JEOL JEM-2010 transmission electron microscope. The crystalline character and crystal phases of the prepared nanostructure were determined by Rigaku-X-ray powder diffractometer (XRD) with Cu Kα radiation (λ = 1.54178 Å) with Bragg angle ranging from 20 to 80°. Raman spectrum of the prepared sample was recorded by using a "LabRam" J-Y spectrometer with a 514.5 nm argon ion laser. The photoluminesence properties of the prepared samples were evaluated by using Jasco, FP-6500 spectrophotometer with a CCD detector with an excitation wave length of 340 nm. ^{1}H NMR data of catalyzed products were acquired on a Bruker 400 MHz NMR spectrometer with $CDCl_3$ and DMSO-d_6 solvents.

Synthesis of ZnO Nanostructures. 3 M aqueous NaOH was added dropwise in to the 0.2 M zinc acetate dihydrate solution and magnetically stirred for 10 min. Then the resultant solution was transferred in to a sonication bath and sonicated for 2 h (ZN-1)/4 h (ZN-2) in an ultrasonicator (40 kHz, 300 W) and a pH of 13 was maintained throughout the course of reactions. Then the obtained white precipitate was filtered, washed several times with methanol to remove the ionic impurities and finally dried at room temperature.

Catalytic Activity of ZnO Nanostructures. Formic acid (0.116 mL, 3 mmol) was gradually added into an amine (1 mmol) with the flower shaped ZnO nanostructures (1 mmol) and magnetically stirred at 70 °C. The progress of a reaction was monitored by TLC. After the completion of a reaction, the mixture was diluted with ethyl acetate. Then the catalyst was filtered and removed from the reaction mixture. The filtrate was washed with 10% $NaHCO_3$ solution and dried with anhydrous Na_2SO_4.

Analytical Data.

Entry 1, *N*-Phenylformamide: ^{1}H NMR (400 MHz, $CDCl_3$) δ 8.64 (s, 1H, -CHO), 7.12-7.65 (m, 5H, Ar-H), 5.21 (s, 1H, -NH).

Entry 2, *N*-(4-Chlorophenyl)formamide: ^{1}H NMR (400 MHz, $CDCl_3$) δ 8.08 (s, 1H, -CHO), 7.10-7.42 (m, 4H, Ar-H), 5.18 (s, 1H, -NH).

Entry 3, *N*-(4-Methoxyphenyl)formamide: ^{1}H NMR (400 MHz, $CDCl_3$) δ 8.30 (s, 1H, -CHO), 7.57 (d, J = 8.3 Hz, 2H, Ar-H), 7.05 (d, J = 8.5 Hz, 2H, Ar-H), 5.45 (s, 1H, -NH), 3.85 (s, 3H, $-OCH_3$).

Entry 4, *N*-(4-Methylphenyl)formamide: ^{1}H NMR (400 MHz, $CDCl_3$) δ 8.52 (s, 1H, -CHO), 7.65 (d, J = 8.8 Hz, 2H, Ar-H), 7.05 (d, J = 8.7 Hz, 2H, Ar-H), 4.93 (s, 1H, -NH), 2.32 (s, 3H, $-CH_3$).

Entry 5, *N*-(3-Methylphenyl)formamide: ^{1}H NMR (400 MHz, $CDCl_3$) δ 8.44 (s, 1H, -CHO), 6.91-7.48 (m, 4H, Ar-H), 5.03 (s, 1H, -NH), 2.32 (s, 3H, $-CH_3$).

Entry 6, *N*-(2-Bromophenyl)formamide: ^{1}H NMR (400 MHz, $CDCl_3$) δ 8.43 (s, 1H, -CHO), 6.93-8.22 (m, 4H, Ar-H), 4.82 (s, 1H, -NH).

Entry 7, *N*-(3-Bromophenyl)formamide: ^{1}H NMR (400 MHz, $CDCl_3$) δ 8.51 (s, 1H, -CHO) 7.01-7.83 (m, 4H, Ar-H), 4.58 (s, 1H, -NH).

Entry 8, *N*-(4-Bromophenyl)formamide: ^{1}H NMR (400 MHz, $CDCl_3$) δ 8.37 (s, 1H, -CHO), 6.91-7.47 (m, 4H, Ar-H), 5.05 (s, 1H, -NH).

Entry 9, *N*-(2-Hydroxyphenyl)formamide: ^{1}H NMR (400 MHz, $CDCl_3$) δ 8.90 (s, 1H, -CHO), 6.33-7.88 (m, 4H, Ar-H), 5.12 (s, 1H, -OH), 4.52 (s, 1H, -NH).

Entry 10, *N*-(2-Cyanophenyl)formamide: ^{1}H NMR (400 MHz, $CDCl_3$) δ 8.79 (s, 1H, -CHO), 7.31-8.16 (m, 4H, Ar-H), 4.21 (s, 1H, -NH).

Entry 11, *N*-(2-Chlorophenyl)formamide: ^{1}H NMR (400 MHz, $CDCl_3$) δ 8.53 (s, 1H, -CHO), 6.60-8.10 (m, 4H, Ar-H), 4.97 (s, 1H, -NH).

Entry 12, *N*-(3-Nitrophenyl)formamide: ^{1}H NMR (400 MHz, $CDCl_3$) δ 8.60 (s, 1H, -CHO), 7.56-8.92 (m, 4H, Ar-H), 4.38 (s, 1H, -NH).

Entry 13, *N*-(3-Hydroxyphenyl)formamide: ^{1}H NMR (400 MHz, DMSO-d_6) δ 8.72 (s, 1H, -CHO), 6.53-7.45 (m, 4H, Ar-H), 5.53 (s, 1H, OH), 5.46 (s, 1H, -NH).

Entry 14, *N*-(4-Hydroxyphenyl)formamide: ^{1}H NMR

(400 MHz, DMSO-d_6) δ 8.33 (s, 1H,-CHO), 6.50-7.38 (m, 4H, Ar-H), 5.47 (s, 1H, OH), 4.76 (s, 1H, -NH).

Entry 15, *N*-(4-Acetylphenyl)formamide: ^{1}H NMR (400 MHz, $CDCl_3$) δ 8.50 (s, 1H, -CHO), 7.96 (d, J = 7.9 Hz, 2H, Ar-H), 7.82 (d, J = 8.3 Hz, 2H, Ar-H), 5.22 (s, 1H, -NH), 2.43 (s, 3H, -$OCOCH_3$).

Results and Discussion

Morphological Characterizations. Zinc cations and hydroxide anions are generated by the hydration of zinc acetate dihydrate and NaOH, respectively. The zinc cations readily react with hydroxide anions to form $Zn(OH)_4^{2-}$ species, which act as the growth units of ZnO nanostructures. The applied sonication energy converts $Zn(OH)_4^{2-}$ species into pure ZnO nanostructures and the involved sonochemical growth mechanism is given as follows:

$$Zn^{2+} + 4\ OH^- \longrightarrow Zn(OH)_4^{2-} \longrightarrow \quad (1)$$

$$Zn(OH)_4^{2-} \longrightarrow ZnO + H_2O + 2OH^- \longrightarrow \quad (2)$$

Figures 1 and 2 depict the FE-SEM images of synthesized ZnO nanostructures. The sample prepared with 0.2 M of zinc acetate dihydrate and 3 M NaOH solution under 2 h (ZN-1) sonication time yielded shuttle like morphologies as shown in Figure 1. Whereas the sample prepared with 0.2 M of zinc acetate dihydrate and 3 M NaOH solution under 4 h (ZN-2) sonication time yielded *Tageteserecta* flower like shaped ZnO structures as shown in Figures 2(a)-(e). With an increase in the reaction time (4 h), shuttle-like morphologies (Figure 1) were started to adhere and assemble each other in forming flower like morphologies (Figures 2(a)-(e)). It was observed that 4 h was the best reaction time to obtain the monodispersed flower-like morphologies (Figures 2(a)-(e)) and a further increase in the time specifies that the energy is continuously added to the reaction system which coagulated the reaction mixture and inhibited the formation of nanostructures.

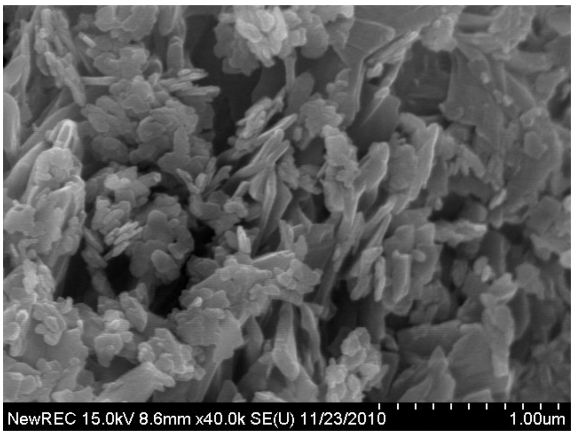

Figure 1. FE-SEM images of ZN-1 sample.

Several tens of hexagonal nanorods constitute a flower like ZnO as shown in highly magnified image of ZN-2 sample (Figure 2(e)). The nanorods are apparently originated from a single centre through their wide bases arranging them in a plane forming flower-like morphologies. It has been observed that all the nanorods of flower like morphologies are radially originated from the center *i.e.*, multiple nanorods growth from center nuclei constitutes the flower like morphologies. The average diameter of a single flower like structure is in the range of 1.8-3 μm. The diameter of nanorods is not homogeneous throughout their lengths and the head and root diameters of nanorods are varied from 120-160 nm. Thus it has been concluded that these nanostructures are formed by the accumulation of several layers and each layer consists of several nanorods. No other morphologies observed from the SEM images ensured the high morphological purity of the prepared sample. The surface areas of prepared flower and shuttle like morphologies are 28 and 16 m^2/g, respectively.

For the detailed morphological characterizations, TEM study was performed for the ZN-2 sample. Figure 3 clearly

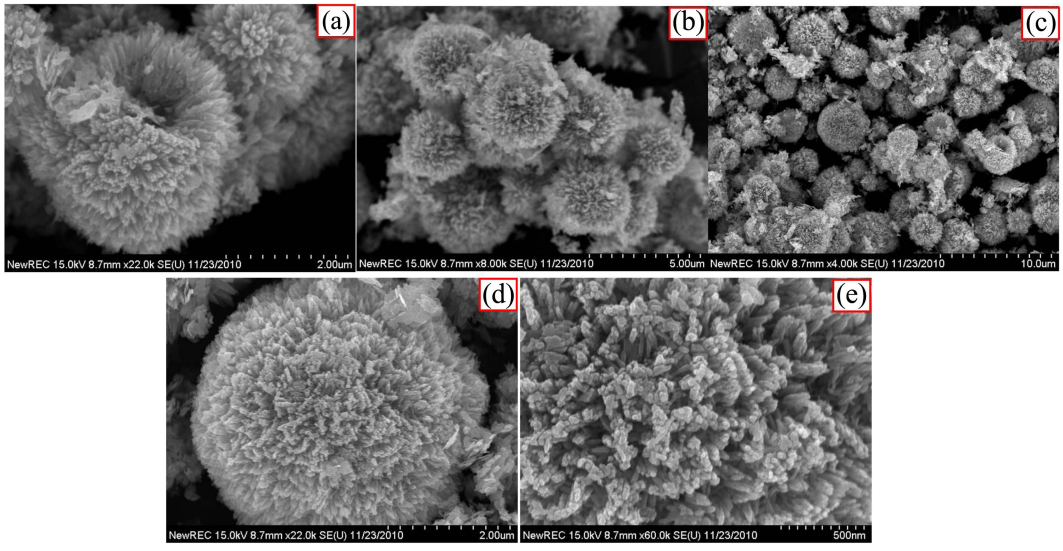

Figure 2. (a-e) FE-SEM images of ZN-2 at different magnifications.

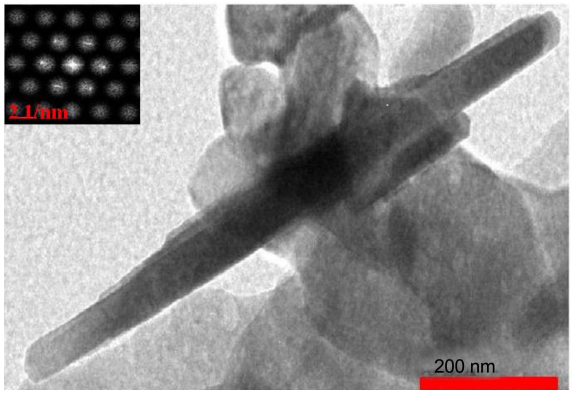

Figure 3. TEM image of ZN-2 sample (inset: SAED pattern).

depicts the nanorod of a flower shaped ZnO and the diameter of a nanorod ranges between 120-160 nm which is consistent with the SEM images. It has been confirmed that the flower shaped ZnO nanostructures are constituted by the accumulation of several nanorods. These nanorods are connected with each other through their bases and constituted the flower like morphologies. The prepared ZN-2 sample was sonicated for the TEM characterization and the sonication process has broken the flower like structure into nanorods which lead to the visualization of a nanorod in the TEM image. The SAED pattern of synthesized ZN-2 sample is given in Figure 3 (inset), the bright spots observed from the Figure ensured the single crystalline nature and the estimated diffraction maxima clearly elucidated the hexagonal phase of the prepared sample.

X-ray Diffraction Studies. The crystallinity and crystal phase of the prepared ZnO nanostructure (ZN-2) was examined by X-ray diffraction (XRD) pattern with Cu-K_α radiation (Figure 4). High crystallinity of the prepared nanostructures was confirmed from the strong intensity and narrow width of the obtained diffraction peaks. The prepared ZnO exhibited the characteristic diffraction patterns at 31.35, 34.25, 36.08, 47.42, 56.39, 62.7, 66.29, 67.82, 69.04, 72.42 and 76.89° and are assigned to the (100), (002), (101), (102), (110), (103), (200), (112), (201), (004) and (202)

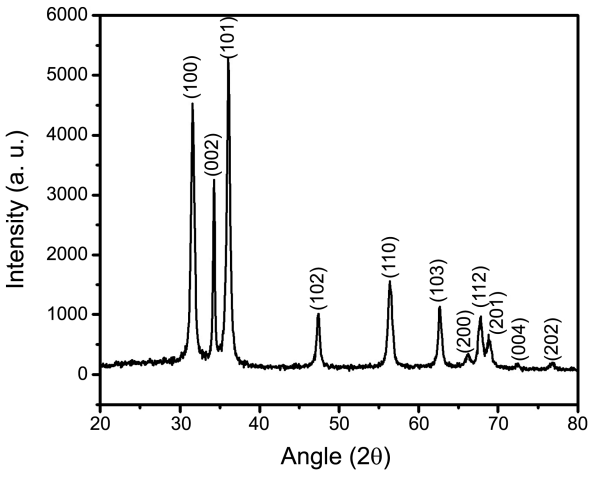

Figure 4. X-ray diffraction pattern of the synthesized ZN-2 sample.

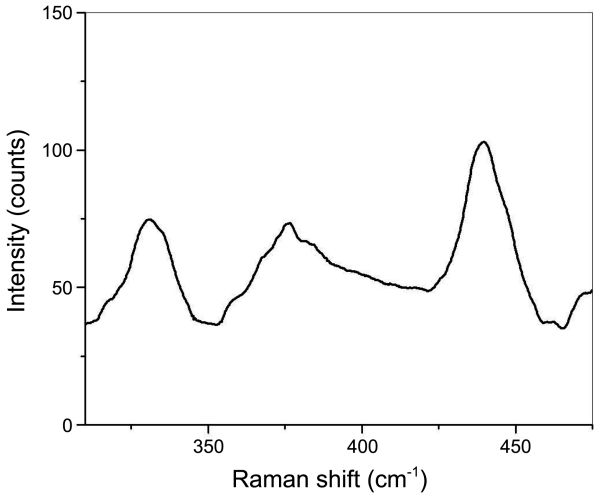

Figure 5. Raman spectrum of the synthesized ZN-2 sample.

facets, respectively. The indexed reflection planes represent the single crystalline wurtzite hexagonal-phase structure (JCPDS Card 75-1526) of ZnO with the unit cell parameters of a=b=3.201 Å and c = 5.2 Å. Except ZnO, no other characteristic peaks were observed in the spectrum, confirming high structural purity of the prepared sample.

Raman Studies. Vibrational properties of the synthesized ZnO nanostructure (ZN-2) was examined by Raman scattering studies at room temperature and depicted in Figure 5. A wurtzite hexagonal phase ZnO belongs to the space group C^4_{6v} with two formula units per primitive cell and all the atoms are occupied in the 2b sites of C_{3v} symmetry. According to group theory, $\Gamma = A_1 + 2B_1 + E_1 + 2E_2$ optic modes exist in the Γ point of the Brillouin zone. Among the mentioned modes, A_1, E_1 and E_2 modes are Raman active. In addition, A_1 and E_1 are infrared active and be splitted into longitudinal optical (LO) components and transverse optical (TO) components.[30] A highly intensified peak observed at 437-439 cm^{-1} is attributed to the Raman active optical-phonon E_2 mode of ZnO crystal. In addition, two more peaks were observed at 331 and 379 cm^{-1} and are attributed to the E_{2H}-E_{2L} (multi-phonon process) and A_{1T} modes, respectively.[31,32] Multiphonon process can occur only for the single crystalline ZnO nanostructures and the obtained spectrum confirmed the single crystalline nature of the prepared nanostructures. A dominant Raman-active E_2 mode observed from the spectrum confirmed the wurtzite hexagonal phase structure[33] of the synthesized ZnO nanostructure with the high crystal quality and structural purity.

Catalytic Activity. To optimize the mole ratio of formic acid and aniline for the better product yield, a control *N*-formylation reaction of formic acid with aniline was carried out at different mole ratios of formic acid and aniline mixture such as 1:1, 2:1 and 3:1. Under the 3:1 molar ratio, a better yield of 60% at 90 min was obtained which is higher than the remaining compositions (data not shown). The yield of *N*-formylation reaction was further enhanced to 89% with an inclusion of 1 mmol ZnO nanocatalyst and the reaction time was also reduced to 30 min (Table 1). The enhanced

Table 1. Flower shaped ZnO nanostructures catalyzed *N*-formylation reactions using formic acid and different amine derivatives at 70 °C

S. No.	Amine	Product	Time (mins.)	Yield (%)
1	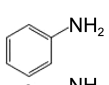	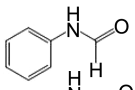	30	89
2	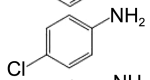	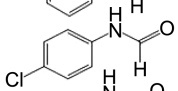	30	84
3	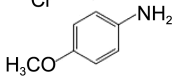	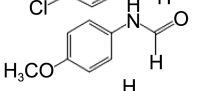	30	83
4	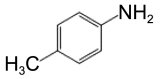	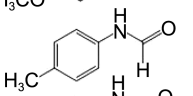	30	86
5	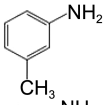	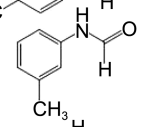	30	83
6	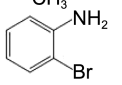	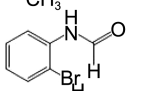	80	79
7	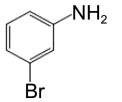	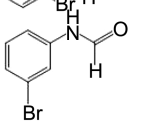	30	82
8	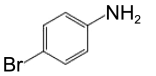	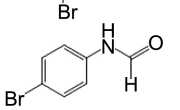	30	86
9	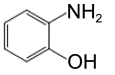	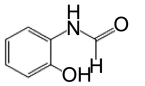	30	83
10	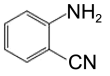	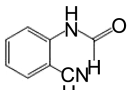	70	75
11	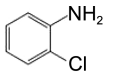	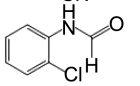	80	79
12	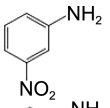	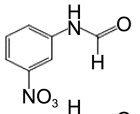	80	76
13	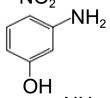	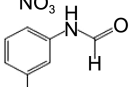	70	85
14	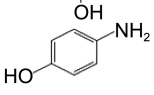	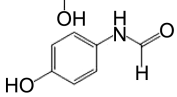	60	86
15	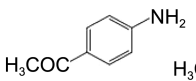	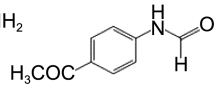	70	80

Reaction conditions: formic acid (3 mmol), amine (1 mmol) and ZnO nanostructures (1 mmol) at 70 °C under solvent free conditions. Yield (%): isolated yields.

output is purely attributed to the high surface area of ZN-2 nanostructures. The enhanced surface area of ZN-2 provides a large area for the adhesion of organic reactants over its surface and increases the contact between the reactants. The number of active sites available in the ZnO nanocatalyst plays a vital role in bringing the reactants at a closer proximity and proper orientation. By the combined efforts of above, the yield of corresponding *N*-formylation reaction

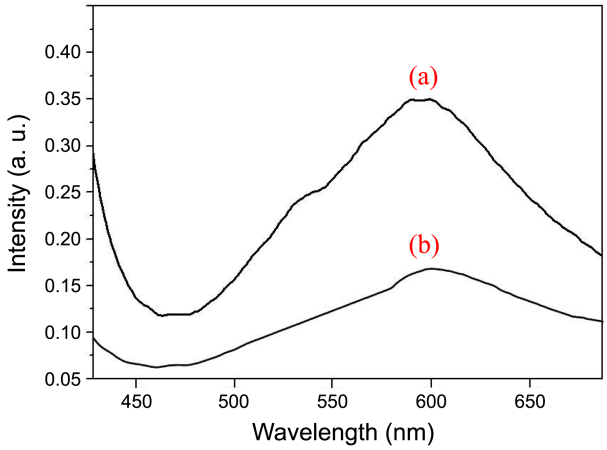

Figure 6. Photoluminescence spectra (a) ZN-1 and (b) ZN-2 nanostructures.

was increased which exhibits the potential catalytic activity of the prepared nanocatalysts. The shuttle like morphologies ZN-1 exhibited a yield of 73% under the similar conditions.

To identify the influential factors which are responsible for the high catalytic activity of flower like ZnO over shuttle like morphologies, PL studies were carried out and shown in Figure 6. The prepared nanostrcutures exhibited a green emission band at 585 nm and is ascribed to the radial recombination of a photo-generated hole with electron of the singly ionized oxygen vacancies in the surface lattices of ZnO. It has also been reported that the radiative transitions between shallow donors (related to oxygen vacancies) and deep acceptors (zinc vacancies) can create defects in the luminescence spectra.[29,30] In addition, the oxygen vacancies occur in three different charge states: the neutral oxygen, singly ionized oxygen and doubly ionized oxygen vacancies. Among these three oxygen vacancies, only the singly ionized oxygen vacancies can act as a luminescence centre. The green emission is ascribed to the recombination of electrons in singly occupied oxygen vacancies in ZnO.[29,30] In general, oxygen vacancies are capable of activating formic acid to form an adsorbed formate anion ($HCOO^-$). Hence, it is clear that oxygen vacancies exist in the ZnO nanostructures are responsible for the formate anion an important intermediate of *N*-formylation reaction and thereby the yield of corresponding product gets enhanced. The flower like ZnO exhibited large amount of oxygen vacancies as evidenced from the PL spectra which favored the yield of corresponding *N*-formylation product over the shuttle like morphologies. The high surface area obtained for the flower like morphologies promoted the number of catalytic active sites which in turn the yield of *N*-formylation product gets enhanced. In addition, flower shaped structures exhibit number of defect states which are also responsible for the high catalytic activities.

The plausible acid catalyzed mechanism for the synthesis of formamide by ZnO nanocatalyst is depicted in Figure 7. The electrophilicity of the carbon atom of carboxylic acid is increased due to the coordination with the ZnO nanocatalyst which facilitate the nucleophilic attack of lone pair of

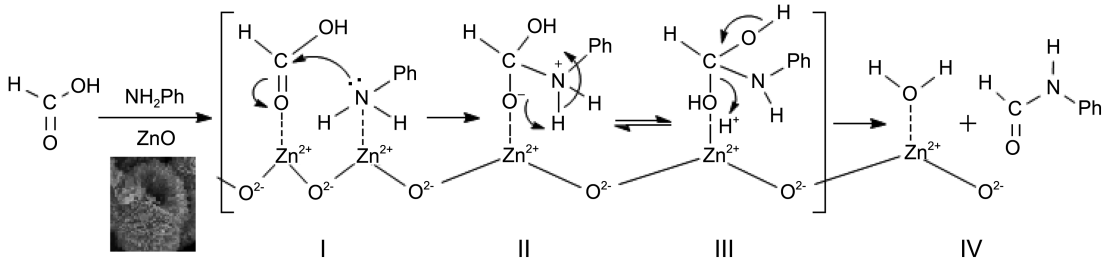

Figure 7. Plausible mechanism of *N*-formylation of amine reaction using ZnO nanostructures.

electrons present in amine to the carbonyl carbon of formic acid (I), which leads to the formation of unstable intermediates. The deprotonation of intermediate (II) and followed by the elimination of water along with the catalyst (III), yielded the desired product (IV).

The scope of this catalytic system was also investigated with the *N*-formylation reactions using formic acid and different amine derivatives with the 3:1 molar ratio under identical conditions and the yield of corresponding products are given in Table 1. It is notable that all the conversions provided the corresponding formamides with the excellent yields at 30-80 min. Amine bearing electron donating groups such as $-CH_3$ and $-OCH_3$ exhibited excellent reaction yields (Table 1, entries 3-5) within a minimal reaction time and is attributed to the increased electron density that they provide in the aromatic system. Meanwhile, electron withdrawing groups such as -CN, $-NO_2$, $-COCH_3$, -Cl and -Br (Table 1, entries 2, 6, 7, 8, 10, 12 and 15) exhibited a lower yield of corresponding products with the prolonged reaction time. The substituents exist at different positions of phenyl ring exhibited an influence on the yield of corresponding amide derivatives. The *para* (Table 1, entries 2 and 8) and *meta* (Table 1, entry 7) substituents were highly reactive over the *ortho* (Table 1, entries 6 and 11) substituents and the lower reactivity of *ortho*-substituted derivatives may be attributed to the steric factors.

Recyclability of catalysts is a vital factor which promotes the competence of green chemistry further. Hence, recyclability tests were carried out for the *N*-formylation control reaction using aniline and formic acid under identical conditions. The catalyst was easily recovered from the mixture by filtration, washed several times with de-ionized water and ethyl acetate and dried under vacuum conditions for 3 h. Then the catalyst was subjected to react with fresh formic acid and aniline reactants. After every reaction, the catalyst was recovered from the reaction mixture and regenerated as described above. Though a gradual yield decrement was observed under repetitive cycles (Figure 8), a prompt yield maintained over the repetitive cycles ensures the potential recyclability behavior of the catalysts. Thus the prepared flower like ZnO nanostructures effectively satisfied the essential requirements of catalysts such as high catalytic activity and excellent recyclability behavior which ensures its potential applications in *N*-formylation reactions.

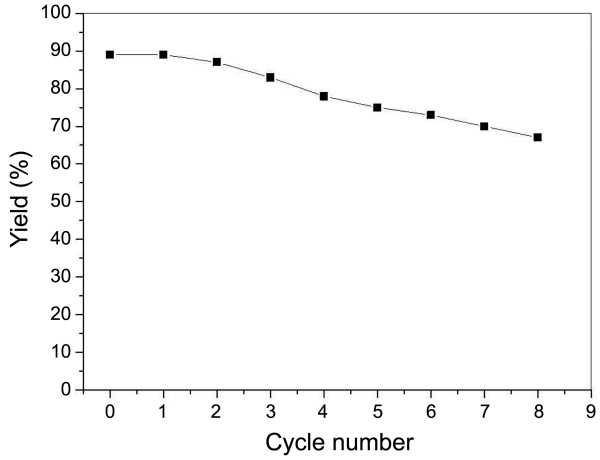

Figure 8. Recyclability behavior of the synthesized ZN-2 nanostructures in *N*-formylation reaction using aniline and formic acid as reactants.

Conclusion

Flower like ZnO nanostructures were synthesized with the aid of an ultrasonication technique without employing any metal catalysts under ambient conditions. The sonication time is a key factor in controlling the texture of the prepared nanostructures. X-ray diffraction pattern ensured the high crystalline character and a wurtzite hexagonal phase of the prepared ZnO nanostructures. The prepared ZnO nanostructures exhibited excellent catalytic activity and recyclability behavior in the *N*-formylation reactions which promise the applications of flower like ZnO nanostructures in catalytic organic reactions field.

Acknowledgments. This paper was supported by research funds of Chonbuk National University in 2013. This research was supported by Basic Science Research Program through the NRF funded by the Ministry of Education, Science and Technology (2011-0010538).

References

1. Jackson, A.; Meth-Cohn, O. *J. Chem. Soc., Chem. Commun.* **1995**, 1319-1319.
2. Chen, B.-C.; Bednarz, M. S.; Zhao, R.; Sundeen, J. E.; Chen, P.; Shen, Z.; Skoumbourdis, A. P.; Barrish, J. C. *Tetrahedron Lett.* **2000**, *41*, 5453-5456.
3. Kobayashi, K.; Nagato, S.; Kawakita, M.; Morikawa, O.; Konishi, H. *Chem. Lett.* **1995**, *24*, 575-576.

4. Kakehi, A.; Ito, S.; Hayashi, S.; Fujii, T. *Bull. Chem. Soc. Jpn.* **1995**, *68*, 3573-3580.
5. Downie, I. M.; Earle, M. J.; Heaney, H.; Shuhaibar K. F. *Tetrahedron* **1993**, *49*, 4015-4034.
6. Han, Y.; Cai, L. *Tetrahedron Lett.* **1997**, *38*, 5423-5426.
7. Bagnall, D. M.; Chen, Y. F.; Zhu, Z.; Yao, T.; Koyama, S.; Shen, M. Y.; Goto, T. *Appl. Phys. Lett.* **1997**, *70*, 2230-2232.
8. Service, R. F. *Science* **1997**, *276*, 895-896.
9. Ryu, Y. R.; Zhu, S.; Budai, J. D.; Chandrasekhar, H. R.; Miceli, P. F.; White, H. W. *J. Appl. Phys.* **2000**, *88*, 201-204.
10. Huang, M. H.; Mao, S.; Feick, H.; Yan, H.; Wu, Y.; Kind, H.; Weber, E.; Russo, R.; Yang, P. *Science* **2001**, *292*, 1897-1899.
11. Umar, A.; Hajry, A. A.; Henit, S. A.; Hahn, Y. B. *J. Nanosci. Nanotechno.* **2008**, *8*, 1-6.
12. Tokumoto, M. S.; Pulcinelli, S. H.; Santilli, C. V.; Briois, V. *J. Phys. Chem. B* **2003**, *107*, 568-574.
13. Lao, J. Y.; Huang, J. Y.; Wang, D. Z.; Ren, Z. F. *Nano Lett.* **2003**, *3*, 235-238.
14. Kong, X. Y.; Ding, Y.; Yang, R. S.; Wang, Z. L. Science **2004**, *303*, 1348-1351.
15. Zheng, Y.; Cheng, Y.; Wang, Y.; Bao, F.; Zhou, L.; Wei, X.; Zhang, Y.; Zheng, Q. *J. Phys. Chem. B* **2006**, *110*, 3093-3097.
16. Firooz, A. A.; Mahjoub, A. R.; Khodadadi, A. A. *Mater. Chem. Phys.* **2009**, *115*, 196-199.
17. Raula, M.; Rashid, M. H.; Paira, T. K.; Dinda, E.; Mandal, T. K. *Langmuir* **2010**, *26*(11), 8769-8782.
18. Zahang, H.; Yang, D.; Li, D.; Ma, X.; Li, S.; Que, D. *Cryst. Growt. & Design.* **2005**, *5*, 547-550.
19. Studenikin, S. A.; Golego, N.; Cocivera, M. *J. Appl. Phys.* **1998**, *84*, 2287-2294.
20. Li, W.; Mao, D. S.; Zheng, Z. H.; Wang, X.; Liu, X. H.; Zhu, S. C.; Li, Q.; Xu, J. F. *Surf. Coat. Technol.* **2000**, *128*, 346-350.
21. Sun, Y.; Fuge, G. M. *Chem. Phys. Lett.* **2004**, *396*, 21-26.
22. Suslick, K. S.; Choe, S. B.; Cichowlas, A. A.; Grinstaff, M. W. *Nature* **1991**, *353*, 414-416.
23. Gao, T.; Wang, Q. *Chem. Mater.* **2005**, *17*, 887-892.
24. Nitani, H.; Yuya, M.; Ono, T.; Nakagawa, T.; Seino, S.; Okitsu, K.; Mizukoshi, Y.; Emura, S.; Yamamoto, T. *J. Nanopart. Res.* **2006**, *8*, 951-958.
25. Banerjee, P.; Chakrabarti, S.; Maitra, S.; Dutta, B. K. *Ultrason. Sonochem.* **2012**, *19*, 85-93.
26. Chen, S.; Kumar, R. V.; Gedanken, A.; Zaban, A. *Isr. J. Chem.* **2001**, *41*, 51-54.
27. Kumar, R. V.; Elgamiel, R.; Koltypin, Y.; Norwig, J.; Gedanken, A. *J. Cystal. Growth.* **2003**, *250*, 409-417.
28. Zhang, Y.; Shi, E. W.; Chen, Z. Z.; Xiao, B. *Mater. Lett.* **2008**, *62*, 1435-1437.
29. Hu, X. L.; Zhu, Y. J.; Wang, S. W. *Mater. Chem. Phys.* **2004**, *88*, 421-426.
30. Rajalakshmi, M.; Arora A. K.; Bendre, B. S.; Mahamuni, S. *J. Appl. Phys.* **2000**, *87*, 2445-2448.
31. Vanheusden, K.; Seager, C. H.; Warren, W. L.; Tallant, D. R.; Voigt, J. A. *J. Appl. Phys.* **1996**, *79*, 7983-7990.
32. Wei, H.; Wu, Y.; Lun, N.; Hu, C. *Mater. Sci. Eng. A* **2005**, *393*, 80-82.
33. Xing, Y. J.; Xi, Z. H.; Xue, Z. Q.; Zhang, X. D.; Song, J. H.; Wang, R. M.; Xu, J.; Song, Y.; Zhang, S. L.; Yu, D. P. *Appl. Phys. Lett.* **2003**, *83*, 1689-1691.